INSTITUTE OF PHYSICS PUBLISHING SMART MATERIALS AND STRUCTURES
Smart Mater. Struct. **14** (2005) 354–362 doi:10.1088/0964-1726/14/2/009

Strain development in curing epoxy resin and glass fibre/epoxy composites monitored by fibre Bragg grating sensors in birefringent optical fibre

E Chehura[1], A A Skordos[2], C-C Ye[1], S W James[1], I K Partridge[2] and R P Tatam[1]

[1] Optical Sensors Group, Centre for Photonics and Optical Engineering, School of Engineering, Cranfield University, Cranfield, Bedford MK43 0AL, UK
[2] Advanced Materials Department, School of Industrial and Manufacturing Sciences, Cranfield University, UK

E-mail: r.p.tatam@cranfield.ac.uk

Received 1 December 2003, in final form 28 October 2004
Published 15 February 2005
Online at stacks.iop.org/SMS/14/354

Abstract
Fibre Bragg gratings (FBGs) fabricated in linearly birefringent fibres were embedded in glass fibre/epoxy composites and in the corresponding unreinforced resin to monitor the effective transverse strain development during the cure process. The optical fibres containing the FBG sensors were aligned either normal or parallel to the reinforcement fibres in unidirectional glass fibre/epoxy prepregs. The chemical cure kinetics of the epoxy resin system used were studied using differential scanning calorimetry, in order to investigate the correlation between the strain monitoring results and the evolution of the curing reaction. A non-parametric cure kinetics model was developed and validated for this purpose. The effective transverse strain measured by the FBGs demonstrated high sensitivity to the degree of cure as a result of the densification of the resin caused by the curing reaction. The effective compressive transverse strain developed during the reaction, and thus the corresponding sensitivity to chemical changes, was higher in the case of the sensing fibre aligned normal to the reinforcement fibres than in the case of the sensor fibre parallel to the reinforcement fibres. Small but measurable sensitivity to cure induced changes was observed in the case of the unreinforced resin.

1. Introduction

Fibre Bragg grating (FBG) sensors are a powerful measurement tool that can perform internal and surface monitoring of strain and temperature, useful in manufacturing processes, impact and damage detection, and structural health monitoring.

The advantages of FBG sensors include their chemical inertness, light weight, and small size (typically 80–125 μm in diameter), which minimizes degradation to the structure caused by the inclusion of the sensor. The measurand is wavelength encoded which permits sensor wavelength-multiplexing, necessary if measurements are required in more than one location.

An important area of application of FBG sensors is in embedded structures where they can be used for structural health monitoring through the lifetime of the structure: from cure monitoring during the production process of composite materials [1] through to in-service health monitoring [2] of the finished product. Composite materials undergo regimes of expansion and shrinkage during the cure process caused by a combination of temperature and chemical/material state changes. The state of residual strain in the final composite part as well as the development of internal stress during the curing

process has a significant effect on the quality of the finished product. In this context, monitoring techniques capable of following internal stress and strain in real time using fibre optic sensors become very useful quality control tools in advanced composite manufacturing. Research in the field has been focused mainly on the measurement of a wavelength shift which has been attributed to longitudinal strain, and temperature using FBG sensors fabricated in single mode (SM) fibre [3–5]. The effects of temperature are often compensated using, for example, a reference grating. In this approach the contribution to wavelength shift due to transverse strain cannot be experimentally measured or separated from longitudinal strain contributions.

FBG sensors fabricated in highly linearly birefringent (HiBi) fibre have been proposed as a solution for multi-axial strain sensing [6]. In this case, a single FBG written in HiBi fibre produces effectively two sensors at the same location but with their transverse strain sensitivities oriented predominantly orthogonally along the two polarization axes of the fibre. Such sensors are ideal for transverse strain measurement. Previous efforts have been limited primarily to theoretical [7, 8] and finite element [9, 10] studies. An experimental demonstration to show how two orthogonally oriented sensors from an FBG written in HiBi fibre respond to transverse load in curing composites has been reported [11, 12]. This work provided evidence of transverse strain development during the cure process from changes in the FBG spectra. There have been a few reports of characterization of the transverse strain response of HiBi FBG sensors through application of known loads [13–16] but these studies do not predict the behaviour when the sensor is deployed in embedded configurations. More research is required in order to determine the actual transverse strains produced by such loading, particularly in real embedded configurations.

This paper presents the first attempt to monitor experimentally the curing process of glass fibre composites and neat resins with FBG sensors written in HiBi (bow tie) fibre using an FBG demodulation system published recently by us [15] and outlined in section 3. These FBGs have been used to monitor the effective strain transverse to the longitudinal axis of the HiBi fibre by neglecting the presence of possible shear strain. It is expected that shear strain will be small during the initial curing, and gelation stages but may be more significant during and post-vitrification. For the work reported here, the main objective was to investigate the feasibility of the use of HiBi FBG sensors to follow and reveal the chemical resin shrinkage during the cure cycle, and to relate these measurements to the evolution of the curing material state as predicted by validated cure kinetics models.

2. Sensor principle

An FBG is a periodic modulation of the refractive index within the core of an optical fibre and acts to couple a forward propagating fibre core mode to a backward propagating core mode at a particular wavelength given by

$$\lambda_B = 2n_{\text{eff}}\Lambda \tag{1}$$

where λ_B, n_{eff}, and Λ are the reflected Bragg wavelength, effective refractive index, and the grating period respectively. A change in the effective refractive index and/or the grating period will cause a shift in the reflected Bragg wavelength. This is the measuring principle upon which physical quantities such as strain, temperature, force, and pressure can be measured by the FBG.

The fabrication of an FBG in HiBi fibre results in two Bragg peaks with centre wavelengths whose separation is typically 0.5 nm in the two polarization axes of the fibre. Each Bragg peak satisfies the form of equation (1). Equations (2) and (3) [8] govern the wavelength response of the HiBi FBG sensor to strain and temperature when shear strain and cross-sensitivity in sensor response are neglected. The equations therefore indicate a linear response. This assumption is justifiable over practical strain and temperature ranges [17, 18]. Experiments on the calibration of HiBi FBG sensitivity to transverse strain have shown very high linear correlation [9, 16]. This shows that the FBG response to transverse strain is linear, which suggests that the effect of cross-sensitivity between the transverse directions may be neglected with minimum penalty.

$$\lambda_s = \lambda_{B,s}\{1 + \varepsilon_a - \tfrac{1}{2}n_0^2[p_{11}\varepsilon_s + p_{12}(\varepsilon_a + \varepsilon_f)] + (\alpha_{0,s} + \xi_{0,s})T\} \tag{2}$$

$$\lambda_f = \lambda_{B,f}\{1 + \varepsilon_a - \tfrac{1}{2}n_0^2[p_{11}\varepsilon_f + p_{12}(\varepsilon_a + \varepsilon_s)] + (\alpha_{0,f} + \xi_{0,f})T\} \tag{3}$$

where λ_i and $\lambda_{B,i}$ ($i = s, f$) are the new wavelengths and the original wavelengths respectively in the slow (s) and fast (f) axes of the fibre. The constants p_{11} and p_{12} are the Pockels strain-optic coefficients, $\alpha_{0,i}$ ($i = s, f$) are the thermal expansion coefficients, $\xi_{0,i}$ ($i = s, f$) are the thermo-optic coefficients in the transverse directions, n_0 is the average refractive index along the two orthogonal eigenaxes of the fibre, T is the temperature of the fibre, and ε_i ($i = a, s, f$) are the normal strain components in the axial and slow and fast axis directions respectively. These relations can be simplified to represent wavelength shifts, $\Delta\lambda_s$ and $\Delta\lambda_f$, in the slow and fast axes respectively. Both equations have an axial strain term. The strain contribution due to temperature can be compensated for in both equations, given the temperature history of the sensor measured by other means, e.g. a thermocouple. The two equations will therefore be considered to have three unknowns. The equations are subtracted to give an effective strain that is still transverse to the longitudinal axis of the fibre (equation (4)). This is still useful for resin cure monitoring experiments that are focused mainly on following the reaction in order to show the various stages of the cure process. The axial strain term, which is common to both equations, is lost through subtraction. The effective transverse strain is therefore given by

$$\varepsilon_f - \varepsilon_s = \frac{2}{n_0^2(p_{12} - p_{11})}\left[\frac{\Delta\lambda_f}{\lambda_{B,f}} - \frac{\Delta\lambda_s}{\lambda_{B,s}}\right]. \tag{4}$$

3. Sensor interrogation system

A schematic diagram of the experimental system for FBG interrogation is shown in figure 1 [15]. The output from a broad bandwidth super-luminescent diode (SLD) with a

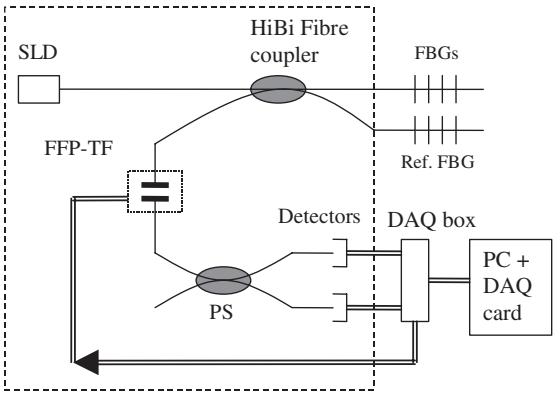

Figure 1. Schematic diagram of the interrogation system. SLD, super luminescent diode; PM FFP-TF, scanning HiBi fibre coupled Fabry–Perot tunable filter; PS, fibre polarization splitter; DAQ, data acquisition.

HiBi fibre pigtail is coupled into the FBG sensors through a 2 × 2 HiBi fibre coupler. The reflected signals pass through a HiBi coupled scanning fibre Fabry–Perot filter (PM FFP-TF, Micron Optics), and are subsequently split into the two orthogonal linear polarization components using a fibre polarization splitter (PS). The spectra of the two orthogonally polarized reflected signals from the FBG sensors written in HiBi fibre are recorded separately using two detectors, and processed in a computer via a data acquisition (DAQ) card and software analysis built on LabView^{TM}.

The SLD has a 3 dB bandwidth of 50 nm centred at 1560 nm and the measured power at the output of the fibre pigtail is 0.6 mW. The DAQ card provides an analogue signal that drives the scanning FFP filter. The FFP filter has a finesse of 895 and free spectral range of 5330 GHz (∼42.7 nm). All components in the interrogation system are connected using Panda fibre (Fujikura) and HiBi FC/PC connectors. The connection between the SLD pigtail fibre and the input arm of the fibre coupler is aligned so that the output powers from the slow and fast axes are approximately equal in each output arm of the coupler. The overall extinction ratio of the interrogation system is measured to be 15 ± 0.5 dB. The PM FFP-TF, HiBi fibre coupler and PS are attached to an aluminium block that is thermally stabilized at a temperature of 25 ± 0.5 °C. All measurements of the wavelength are made relative to a thermally stabilized FBG at a temperature of 25 ± 0.5 °C. This system offers independent and simultaneous real-time detection of the two orthogonally polarized signals reflected from FBG sensors in HiBi fibre, thus allowing automated operation. There is no limitation on the measurable strain imposed by the resolution of the orthogonally polarized Bragg peaks.

4. Experimental details

The epoxy resin used in this study was a commercial multifunctional epoxy system cured with a dicyandiamide hardener; this is representative of the class of high performance epoxies utilized in current aircraft composite structures. The chemical cure kinetics information was gathered using a heat flux differential scanning calorimeter (DSC) [19]. Dynamic cure experiments were carried out at 0.5, 1, 2, 4, 6, 8, 10, 15, and 20 °C min^{-1} and isothermal experiments between 70 and 130 °C in 5 °C intervals. The samples were encapsulated in aluminium pans. An empty pan was placed on the reference side of the instrument. After equilibrating the DSC cell at 60 °C the thermal program was imposed, by following the required heating rate in the case of dynamic experiments or by jumping to the cure temperature using a heating rate of 20 °C min^{-1} in the case of isothermal experiments. The mass of the samples was kept between 4 and 6 mg, in order to ensure negligible thermal gradients, and all experiments were duplicated.

FBG sensors were fabricated, in our laboratories, in HiBi fibre (Fibercore HB1500) at centre wavelengths in the 1550 nm region. The HiBi fibre was pressurized to 150 bars in hydrogen for a period of two weeks before the FBG inscription. Each FBG that was fabricated resulted in two Bragg peaks separated by 0.35 nm in the two polarization axes of the fibre. The FBGs were annealed at 200 °C for about 4 h to ensure that the wavelength was stabilized against thermal related decay in refractive index modulation.

FBG cure monitoring experiments of unidirectional glass fibre/epoxy composites and of neat resins were performed using the configuration illustrated in figure 2. The glass fibre prepreg was cut into layers measuring 25 mm × 15 mm to fit into a heated copper cylinder with a rectangular opening of similar dimensions. The cylinder was surrounded by heating elements controlled by a Eurotherm temperature controller. Smaller specimens were preferred in order to have a more accurate temperature control of the cure profile by minimizing thermal lag between the heating tool and the HiBi FBG embedded in the middle of the specimen. The cylindrical geometry of the heating tool provided a more uniform heat distribution on the specimen. The proximity of the specimen boundaries of such relatively small specimen sizes to the embedded FBG is therefore considered to have insignificant influence on the measurements. The temperature of the heating element was measured using a thermocouple placed in an opening on the wall of the hollow cylinder. A second thermocouple was placed in the rectangular opening in contact with the curing material in order to record the actual thermal profile followed by the resin. The HiBi fibre containing the FBG sensors was embedded in the uncured composite coupon. In all experiments, the slow axis of each of the HiBi FBG sensors was aligned in the plane of the material (figure 2). The axes of the HiBi fibre were identified through observation of the diffraction pattern from the fibre when illuminated from the side with a helium neon laser source [20]. The translation stages in figure 2 were used for fixing the HiBi optical fibre containing the FBGs and could be used to pre-strain the FBG so that any possible compressive axial loads during the initial stages of the cure process could also be detected.

One experiment was carried out with a HiBi FBG sensor embedded in a glass fibre composite and aligned normal to the reinforcement fibres. The FBG sensor was embedded into an eight-layer composite coupon, four layers below the top layer, such that the optical fibre was normal to the reinforcement fibres. Prior to cure, pressure was applied to the specimen in the out-of-plane direction, but the specimen was left unconstrained in the axial direction.

The next experiment was carried out with a HiBi FBG sensor embedded in a glass fibre composite and aligned parallel

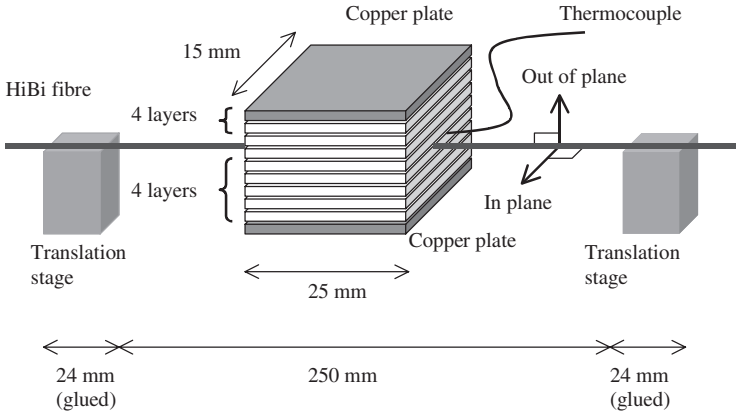

Figure 2. Schematic diagram showing the experimental configuration of the cure monitoring experiments and the alignment of the polarization axes of the HiBi fibre in the material.

to the reinforcement fibres. The HiBi fibre was sandwiched between layers 6 and 7 of the eight-layer composite (figure 2). The specimen was left unconstrained from the top as well as in the axial direction.

A third experiment was performed with a HiBi FBG sensor embedded in neat resin. The purpose of this experiment was to assess the effect of the presence or absence of the reinforcement fibres in the resin on the FBG sensor response. The specimen was sandwiched between two copper plates spaced by Teflon that acted as a releasing agent to allow free movement of the sample from the copper plates during the cure. Pressure was applied initially to the specimen in the transverse direction but the axial direction was left unconstrained. The FBG sensor was aligned such that the slow axis lay in the plane of the specimen.

In all cases the cure was performed at a temperature of about 100 °C. The temperature was increased linearly up to the cure temperature within 5–10 min and then maintained at a constant value until completion of the cure. As the geometry of the experimental set-up imposed a thermal lag between the control temperature and the actual temperature in the curing material, which was not absolutely reproducible over different experiments, slight variations in the actual thermal profiles were observed. The use of an appropriate cure kinetics model, discussed in the following section, removes any limitations imposed by this fact on the comparative interpretation of the results: the comparison is carried out on the basis of material state as characterized by the degree of cure.

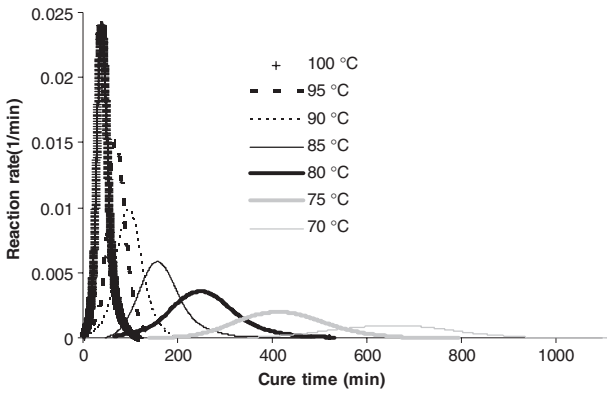

Figure 3. Reaction rate versus time in low temperature isothermal DSC cure experiments.

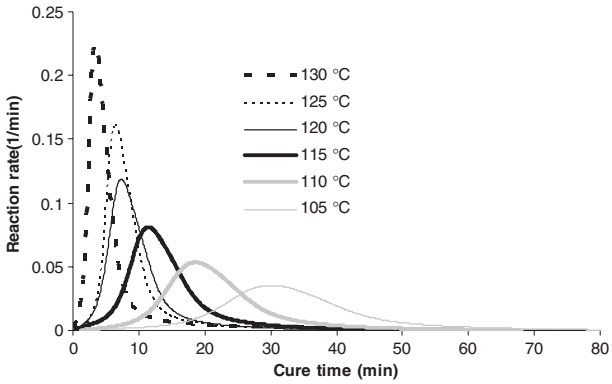

Figure 4. Reaction rate versus time in high temperature isothermal DSC cure experiments.

5. Cure kinetics results and modelling method

The raw DSC signals were transformed to cure kinetics information by assuming that the reaction rate was connected to the heat release rate with a proportionality relation and by using an appropriate algorithm for the integration of the heat flow curve. The integration algorithm used for the dynamic heating runs was proposed by Bandara [21] and constitutes an iterative determination of a baseline that fits the initial and final slopes of the DSC signal and changes gradually from one to the other at intermediate points. The integration of isothermal DSC traces was performed using a horizontal baseline tangential to the end plateau of the reaction signal. The need for this type of baseline was dictated by the experimental conditions that disallowed any adjustment of the baseline, as changes in the specific heat capacity of the resin resulting from the cure should not play any role under isothermal conditions.

The total heats of reaction estimated by the integration of the heat flow curves are given in table 1. The total heat of reaction is 533 ± 13 J g^{-1} and does not depend on the heating rate of the experiment. Knowledge of the total heat of the reaction allows the translation of the DSC data into reaction rate or conversion curves. Figure 3 depicts reaction rate versus

Table 1. Total heat of reaction at different heating rates.

Rate (°C min^{-1})	0.5	1	2	4	6	8	10	15	20	Average	Deviation
Heat (J g^{-1})	530	510	523	525	547	530	540	546	546	533	13

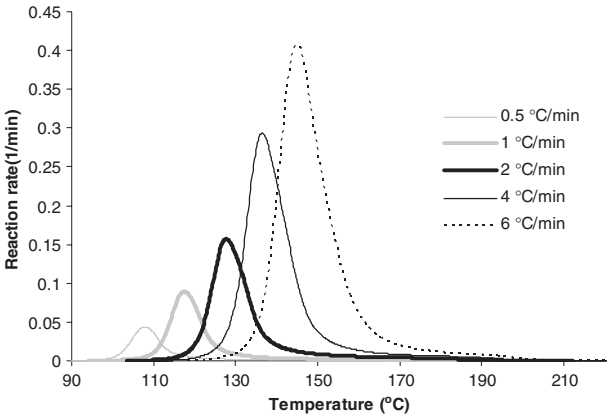

Figure 5. Reaction rate versus time in low heating rate dynamic DSC cure experiments.

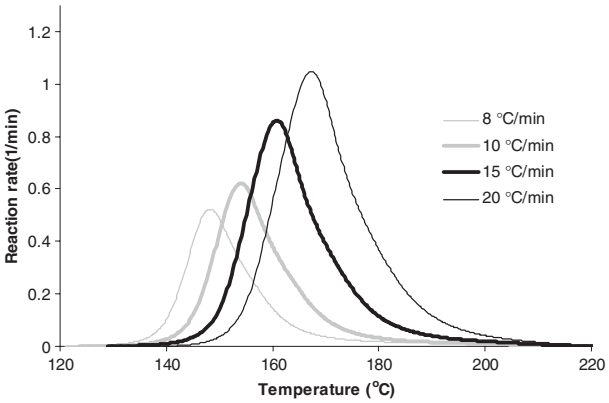

Figure 6. Reaction rate versus time in high heating rate dynamic DSC cure experiments.

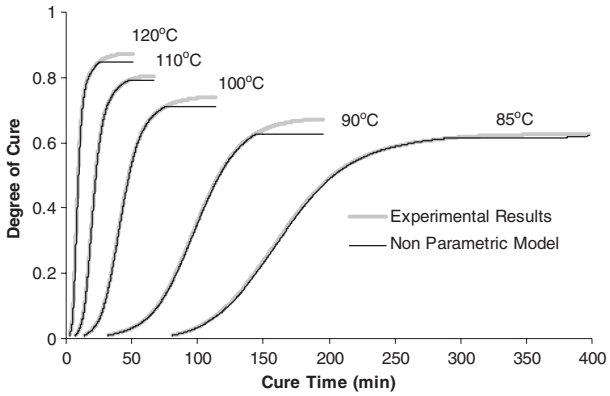

Figure 7. Comparison of cure kinetics model and experimental results under isothermal conditions. —, experimental results; —, non-parametric model.

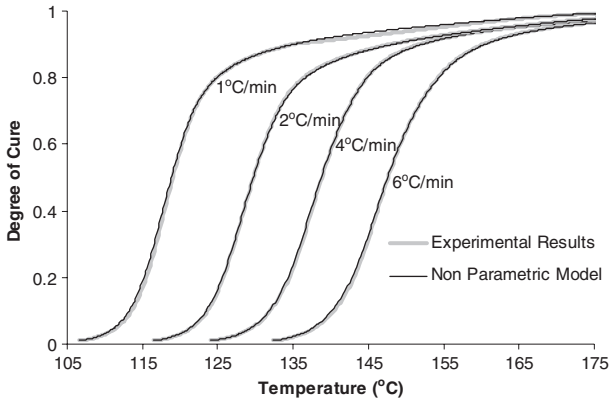

Figure 8. Comparison of cure kinetics model and experimental results under dynamic conditions. —, experimental results; —, non-parametric model.

time curves for low temperature isothermal cures and figure 4 the corresponding data for high temperature isothermal cures. The curves are characteristic of the autocatalytic cure kinetics of the system, with a maximum in reaction rate appearing at intermediate stages of the cure [19]. The reaction duration ranges from 1100 min at 70 °C to 30 min at 130 °C. The results of dynamic runs are given in figures 5 and 6. The reaction under dynamic conditions is dominated by a single peak.

A cure kinetics model of the form of equation (5) is required in order to compute the evolution of the state of the material, as expressed by the degree of cure

$$\frac{\mathrm{d}\alpha}{\mathrm{d}t} = f(\alpha, T). \tag{5}$$

Here α denotes the degree of cure, t the cure time and T the temperature. The aim of cure kinetics modelling is to identify the unknown functional expression. This can be achieved either explicitly by fitting a parametric model to experimental data or by combining experimental data and an interpolation routine into a computer code that accepts a degree of cure–temperature point as an input and returns a value for the reaction rate. The two approaches yield equivalent results when they are based on the same set of experimental data; however, one might be preferred over the other depending on the trade-off between the cost of obtaining a dense set of experimental data and the cost of finding and fitting an appropriate functional expression [22]. The procedure adopted here is that of non-parametric modelling. Details of the model algorithm are given elsewhere [22].

In order to evaluate the performance of the model, which was subsequently used for interpretation of the FBG strain monitoring results, experimental curves obtained by integration of the reaction rate versus time curves are compared with the model results in figures 7 and 8. It can be observed that the non-parametric model follows the results of the experiments very closely. Deviation of the model results from the DSC results is observed only in the latest stages of the cure under isothermal conditions. This can be explained by the operation of the non-parametric model as an interpolation routine that forces a zero reaction rate when the point in the degree of cure–temperature plane at which the reaction rate is

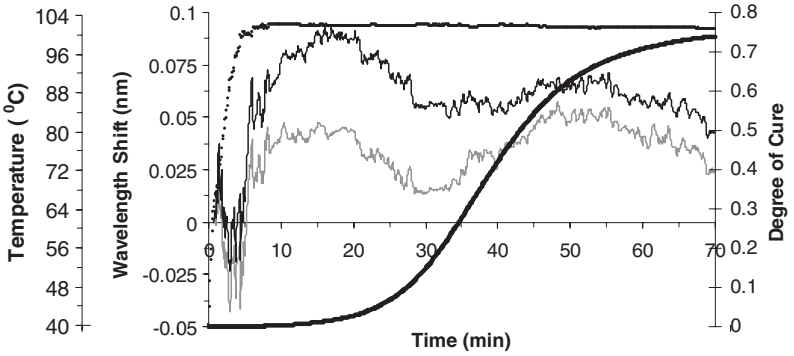

Figure 9. Out-of-plane and in-plane FBG wavelength shifts, temperature, and degree of cure versus time for the experiment with the HiBi fibre normal to the reinforcement fibres. —, FBG wavelength shift measured out of plane; —, FBG wavelength shift measured in plane; —, degree of cure; ●, temperature.

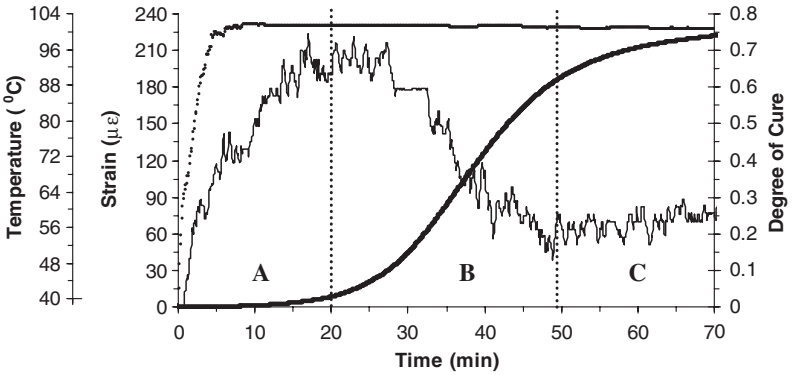

Figure 10. Effective transverse strain, temperature, and degree of cure versus time for the experiment with the HiBi fibre normal to the reinforcement fibres. —, effective transverse strain; —, degree of cure; ●, temperature.

calculated is not enclosed by experimental points. In the case of high degrees of cure in isothermal conditions the experimental curve at a lower temperature does not include the conversion point, and consequently the reaction rate value becomes zero.

6. Cure monitoring results

Figure 9 shows the evolution of the degree of cure as a function of time together with the temperature profile and the wavelength shift of the FBG sensor monitored in both polarization axes of the HiBi fibre. The wavelength shift has been compensated for temperature effects i.e. thermal expansion and thermo-optic effects, combining data from the thermocouple with data obtained from our previously reported characterization of the properties of HiBi FBG sensors [16]. The wavelength shift shows that the wavelength of the FBG in each axis becomes shorter during the initial stages of the cure but the difference between the two is approximately constant, implying no transverse load during this period. The decrease in the wavelength shift may be associated with the release of pressure that was applied initially to the specimen bearing the FBG sensor and to a thermal lag possibly occurring between the thermocouple and the FBG sensor embedded at slightly different spatial locations. When this pressure was applied to the specimen, a Bragg wavelength shift was observed from the FBG sensor. This shift can be reversed when the pressure is relieved through an increase in temperature due to the softening of the material surrounding the FBG sensor. After approximately 5 min the separation between the wavelength shifts increases, implying an increase in the transverse load. The separation between the two decreases after approximately 20 min, signifying a decrease in transverse load. The constant wavelength separation after 50 min means that there is no change to transverse load and this is indicative of a near complete reaction whereby the final state of the material is being defined.

Figure 10 illustrates the degree of cure and temperature alongside the effective transverse strain that was calculated using equation (4). Region A of the figure shows an increase of effective transverse strain ($\sim$210 $\mu\varepsilon$) during which the reaction is still insignificant. This increase in effective transverse strain is therefore largely associated with the thermal expansion of the specimen during heating up and a minor contribution from the release of the pressure applied initially to the specimen. In region B the effective transverse strain decreases by about 160 $\mu\varepsilon$ which can be associated with the curing reaction since it occurs during the fast reaction time regime. The effective transverse strain is approximately constant at 60 $\mu\varepsilon$ in region C of the figure, thus implying a near complete cure reaction. The thermocouple temperature profile was found to be noisy, particularly in the fast reaction time regime, and this was found to be the case in all subsequent experiments described here. The temperature data were therefore smoothed using an adjacent averaging technique before being used in the strain analysis. The noise on the effective transverse strain data was found in all experiments. It may arise from a strain transfer

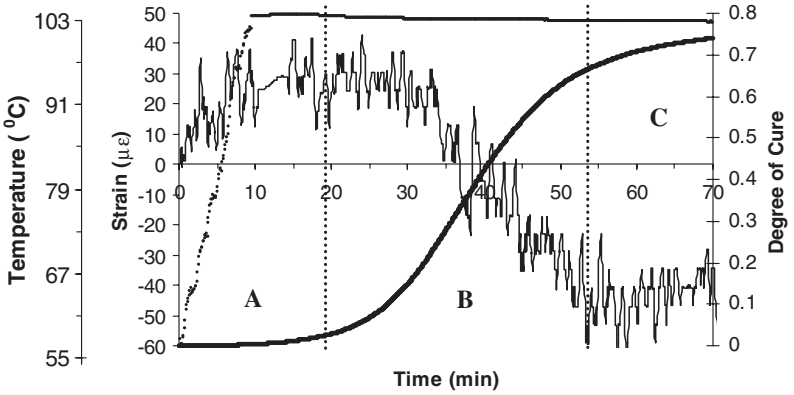

Figure 11. Effective transverse strain, temperature, and degree of cure versus time for the experiment with the HiBi fibre parallel to the reinforcement fibres. —, effective transverse strain; —, degree of cure; ●, temperature.

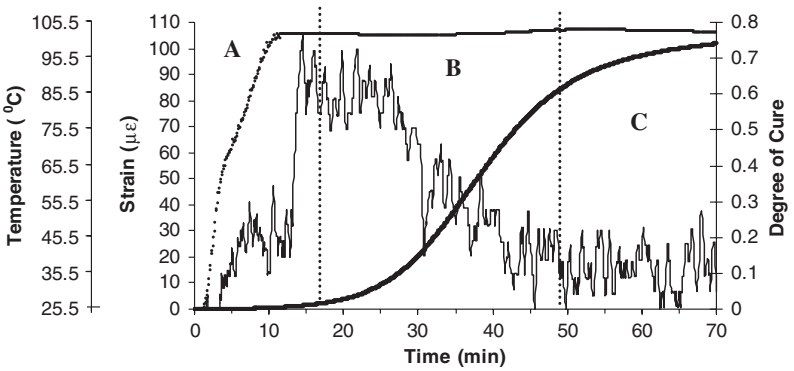

Figure 12. Effective transverse strain, temperature, and degree of cure versus time for the experiment with the HiBi fibre embedded in unreinforced resin. —, effective transverse strain; —, degree of cure; ●, temperature.

coefficient between the fibre and the specimen that is poor, particularly when the specimen is in a liquid state. Also, noise may result from the subtraction of two uncorrelated data sets containing fractional wavelength shifts from orthogonal transverse directions.

The effective transverse strain indicated by measurements from the HiBi fibre containing the FBG sensor arranged parallel to the reinforcing fibres is illustrated in figure 11. The behaviour may be considered to be similar to that observed in the case of the HiBi FBG sensor arranged normal to the reinforcing fibres, but with the curve extending past the initial, quiescent strain to negative strain. The effective transverse strain measured in region A of the figure may be attributed to the thermal expansion of the specimen during heating up. The measured values decreased by about 80 $\mu\varepsilon$ in region B in which the bulk of the cure reaction takes place and this effect is therefore associated with chemical shrinkage. Region C of the figure shows a near constant effective transverse strain (~ -40 $\mu\varepsilon$), signifying a cure reaction that is nearing completion.

Figure 12 depicts the effective transverse strain measurement for a sensor in unreinforced resin. The behaviour is qualitatively identical to the previous case (figure 11). The increase in effective transverse strain in region A of the figure is largely attributed to thermal expansion of the specimen during heating up and a minor contribution from the release of the pressure initially applied to the specimen as discussed before. When the reaction occurs, in region B, the FBG sensor measures a decrease in effective transverse strain of about 70 $\mu\varepsilon$. Region C of the figure shows an effective transverse strain that is approximately constant at 15 $\mu\varepsilon$, thus signifying a near complete cure reaction. The decrease in effective transverse strain measured in region B, as expected, is in agreement with that of the FBG sensor aligned parallel to the reinforcing fibres in the composite (figure 11), for both cases involve a resin rich environment surrounding the FBG sensor.

The relation between effective transverse strain and the progress of the reaction can be ascertained from the correlogram given in figure 13 for the three cases studied here. For clarity, only the points corresponding to the interval of fast reaction were included. It can be observed that in all cases effective transverse strain is a decreasing function of the degree of cure. A linear regression was performed in order to evaluate the quality of the correlation. Although the noise in the FBG signals causes some scattering of the points, the correlation is high. Consequently, the effective transverse strain as calculated using equation (4) successfully follows the chemical shrinkage. The results reported here can be further enhanced by the use of a non-linear relation between the degree of cure and chemical shrinkage. Recent reports in the literature have shown that different resin systems have different behaviour as far as the shrinkage–degree of cure relation is concerned [23, 24]; the use of a model appropriate for this resin system would improve the correlation.

The average sensitivity of the effective transverse strain to the degree of cure as obtained by calculation of the slope of the regression lines for the three cases is given in

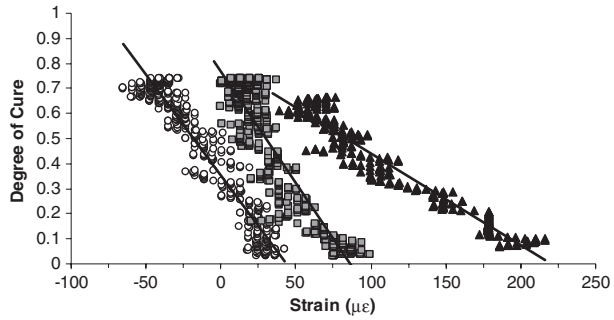

Figure 13. Correlation between progress of cure and effective transverse strain for three experimental cases. ▲, HiBi fibre normal to reinforcement fibres, $R^2 = 0.9546$; ○, HiBi fibre parallel to reinforcement fibres, $R^2 = 0.9239$; □, HiBi fibre embedded in unreinforced resin, $R^2 = 0.8141$.

Table 2. Sensitivity of effective transverse strain measured by the HiBi FBG sensor to degree of cure.

Case	FBG sensor normal to reinforcement fibres	FBG sensor parallel to reinforcement fibres	Isotropic material
Sensitivity ($\mu\varepsilon$)	−280	−120	−100

table 2. The sensitivity coefficients indicate that the response is significantly stronger in the case of the FBG sensor oriented normal to the reinforcing fibres. When the FBG sensor is placed parallel to the reinforcing fibres, the sensitivity is observed to be slightly higher than in the case of isotropic material. These results may be interpreted by consideration of the loading situation around the HiBi fibre during shrinkage. As the geometry of the curing material is planar it is expected that shrinkage will occur as compression in the thickness direction. In the vicinity of the HiBi fibre the material will tend to rearrange itself around the HiBi fibre, at least while the material has not reached a near solid state. The rearrangement will be significantly easier in the case of unreinforced resin, thus resulting in low sensitivity of the sensor response. In addition, reinforcement fibres parallel to the sensor axis find it easier to move during compression than normal fibres, with the result of significantly higher sensitivity in the latter case.

7. Discussion

A full characterization of the state of internal stress for a curing composite requires a complete three-dimensional (3D) strain measurement to be performed. Such an experimental approach would enable the state of residual strain to be fully determined. Simultaneous use of several individual FBG sensors oriented in different directions in the material could be seen as a potential experimental tool to this end. However, such a methodology suffers from the fact that the 3D measurement would not be performed at one location. In addition, potential erroneous measurements may result from fibre to fibre interaction, particularly for fibres placed in close proximity, as previous research has indicated the existence of stress concentrations within four fibre diameters in the vicinity of an embedded fibre [25]. This approach is therefore limited in its applicability.

Localized 3D strain measurements can in principle be performed from measurements in the shift of four different FBG wavelengths if the principal strain directions are known. In this case the four wavelength shifts are induced by the three normal strains and temperature. This can be achieved by gratings in HiBi fibre with sufficiently different strain coefficients and one way is to use two different wavelengths for collocated FBGs. However, if principal strains are not known or if complex strain fields exist in the locality of the fibre this method will not measure 3D strain and additional measurements will have to be made in order to extract shear strain components in addition to the normal components.

8. Conclusions

Effective transverse strains have been measured using FBG sensors written in HiBi fibres in a curing resin and in glass fibre/epoxy composites. The results of strain monitoring experiments were interpreted using a non-parametric model that was applied to the reaction kinetics of the cure process. The effective transverse strain measured was a difference between two normal components but the two components are not separable. The results indicate that the measured effective transverse strain was able to follow both the thermal and the 'chemical' dimensional changes of the epoxy resin by comparing with the cure kinetics model predictions. The measured effective transverse strain showed a very strong correlation with the progress of the reaction, indicating that the technique was able to follow and reveal the chemical resin shrinkage during the cure cycle, as supported by validated cure kinetics models. This preliminary work serves to demonstrate the potential of the technique and provide a platform for further instrument development before it can be utilized for the critical task of chemical shrinkage monitoring during the cure where complete 3D quantitative measurements may be required.

The responsivity of transverse strain to chemical shrinkage depends on the loading situation in the vicinity of the HiBi fibre and consequently is a function of the orientation of the reinforcing fibres in contact with the HiBi fibre containing the FBG sensor. The interpretation of the results has been simplified by assuming that the principal strain axes are known and remain fixed. However, it may be more complex considering the complex loading situation likely to exist in the vicinity of the fibre.

Acknowledgment

This work was supported by the Engineering and Physical Sciences Research Council (EPSRC), UK (GR/M89454).

References

[1] Chen J-Y, Hoa S V, Jen C-K and Wang H 1999 Fibre-optic and ultrasonic measurements for *in situ* cure monitoring of graphite/epoxy composites *J. Compos. Mater.* **33** 1860–81

[2] Whelan M P, Albrecht D and Capsoni A 2002 Remote structural monitoring of the Cathedral of Como using an optical fibre Bragg grating sensor system *Proc. SPIE* **4694** 242–52

[3] Rao Y J 1999 Recent progress in applications of in-fibre Bragg grating sensors *Opt. Laser Eng.* **31** 297–324

[4] James S W, Dockney M L and Tatam R P 1996 Simultaneous independent temperature and strain measurement using in-fibre Bragg grating sensors *Electron. Lett.* **32** 1133–4
[5] Giordano M, Laudati A, Nasser J, Nicolais L, Cusano A and Cutolo A 2004 Monitoring by a single fiber Bragg grating of the process induced chemo-physical transformations of a model thermoset *Sensors Actuators* A **113** 166–73
[6] Udd E, Schulz W, Seim J, Haugse E, Trego A, Johnson P, Bennett T E, Nelson D and Makino A 2000 Multidimensional strain field measurements using fibre optic grating sensors *Proc. SPIE* **3986** 255–62
[7] Sirkis J S and Haslach H W 1991 Complete phase-strain model for structurally embedded interferometric optical fibre sensors *J. Intell. Mater. Syst. Struct.* **2** 3–24
[8] Sirkis J S 1993 Unified approach to phase-strain–temperature models for smart structure interferometric optical fibre sensors: part 1, development *Opt. Eng.* **32** 752–61
[9] Lawrence C M, Nelson D V, Udd E and Bennett T 1999 A fibre optic sensor for transverse strain measurement *Exp. Mech.* **39** 202–9
[10] Lawrence C M, Nelson D V and Makino A 1997 Modeling of multi-parameter Bragg grating sensor *Proc. SPIE* **3180** 42–9
[11] Udd E, Black K, Schulz W, Kreger S, Kunzler M and Heider D 2002 *In situ* evaluation of composite structural performance in presence of high stress/strain gradients using multi-axis fibre grating strain sensors *15th Int. Conf. on Optical Fiber Sensors (Portland OR, USA)* (Piscataway, NJ: IEEE) pp 59–62
[12] Chehura E, Skordos A, Ye C-C, James S W, Partridge I and Tatam R P 2003 Multi-axial strain monitoring in curing glass fibre/epoxy composites measured using fibre Bragg grating sensors fabricated in high birefringent fibres *16th Int. Conf. on Optical Fiber Sensors (Nara, Japan)* (Japan: IEICE) pp 180–3
[13] Udd E, Nelson D and Lawrence C 1997 Multiple axis strain sensing using fiber gratings written onto birefringent single mode optical fibre *12th Int. Conf. on Optical Fiber Sensors (Williamsburg, USA)* (Washington, DC: OSA) pp 48–51
[14] Bosia F, Giaccari P, Facchini M, Botsis J, Limberger H and Salathe R 2002 Characterisation of embedded fiber Bragg grating sensors written in high-birefringent optical fibres subjected to transverse loading *Proc. SPIE* **4694** 175–86
[15] Ye C-C, Staines S E, James S W and Tatam R P 2002 A polarization-maintaining fibre Bragg grating interrogation system for multi-axis strain sensing *Meas. Sci. Technol.* **13** 1446–9
[16] Chehura E, Ye C-C, Staines S E, James S W and Tatam R P 2004 Characterization of the response of fibre Bragg gratings fabricated in stress and geometrically induced high birefringence fibres to temperature and transverse load *Smart Mater. Struct.* **13** 888–95
[17] Farahi F, Webb D J, Jones J D C and Jackson D A 1990 Simultaneous measurement of temperature and strain: cross-sensitivity considerations *J. Lightwave Technol.* **8** 138–42
[18] O'Dwyer M J, Ye C-C, James S W and Tatam R P 2004 Thermal dependence of the strain response of optical fibre Bragg gratings *Meas. Sci. Technol.* **15** 1607–13
[19] Pascault J-P, Sautereau H, Verdu J and Williams R J J 2003 *Thermosetting Polymers* (New York: Dekker) ISBN: 0-8247-0670-6
[20] Pannell C N, Tatam R P, Jones J D C and Jackson D A 1988 A fibre-optic frequency shifter utilising travelling flexure waves in birefringent fibre *J. Inst. Electron. Radio Eng.* **58** (Suppl.) S92–8
[21] Bandara U 1986 A systematic solution to the problem of sample background correction in DSC curves *J. Therm. Anal.* **31** 1063–71
[22] Skordos A A and Partridge I K 2001 Cure kinetics modelling of epoxy resins using a non-parametric numerical procedure *Polym. Eng. Sci.* **41** 793–805
[23] Zarrelli M, Skordos A A and Partridge I K 2002 Investigation of cure induced shrinkage in unreinforced epoxy resin *Plast. Rubber Compos.* **31** 377–84
[24] Li C, Potter K, Wisnom M R and Stringer G 2004 *In situ* measurement of chemical shrinkage of MY750 epoxy resin by a novel gravimetric method *Compos. Sci. Technol.* **64** 55–64
[25] Sirkis J S, Mathews C and Singh H 1990 Optical and mechanical interaction of structurally integrated optical fibre sensors *Proc. SEM Spring Conf.* pp 511–6